# Moisture effects on 4-point bending behavior of GFRP-balsa sandwich by acoustic emission and infrared thermography

Yuan Wu[1], Marianne Perrin[1], Marie-Laetitia Pastor[1], Pascal Casari[2] and Xiaojing Gong[1]

[1]Institut Clément Ader (ICA), CNRS, UMR 5312, Université de Toulouse, 65000 Tarbes, France. E-mail : marianne.perrin@iut-tarbes.fr
[2]Institut de Recherche en Génie Civil et Mécanique, GeM-E3M, CNRS, UMR 6183, Université de Nantes, 44606 Saint Nazaire, France. E-mail: pascal.casari@univ-nantes.fr

**Keywords:** GFRP-balsa sandwich; Moisture effects; Acoustic Emission; InfraRed Thermography.

## 1. Introduction

Composite sandwich structures are widely used for civil, aeronautical and marine applications (Wu Y et al., 2021) due to their good stiffness-to-weight ratio. It consists of two thin but stiff skins bonded to the center thicker but lighter core, thus, skins mainly provide bending stiffness and strength, while the core mainly carries shear stresses. Among various core materials, balsa wood has been widely utilized as the light bio-based core in sandwich structures in construction and marine fields (Shi H et al., 2018), bonded with Glass Fiber Reinforced Polymer (GFRP) skins. However, few researches have been focused on balsa cored sandwich, due to the complex anisotropic properties of wood material and strong dependency of its mechanical performance on density (Da Silva A et al., 2007). Furthermore, balsa wood shows high sensitivity to moisture, raising to the need to characterize moisture effects on mechanical properties of balsa sandwich.

In this work, Non-Destructive Testing (NDT) techniques (Munoz V et al., 2016), including Acoustic Emission (AE) and InfraRed Thermography (IRT), were coupled to investigate the bending behavior and damage mechanisms of GFRP-balsa sandwich structures. Post-mortem examinations by microscope were also compared with NDT observations to characterize the skin and core damages, separately.

## 2. Materials and methods

GFRP-balsa sandwich specimens with special triple dog-bone shape (see Fig. 1. (a)) were designed, to easily observe the possible skin damages in pure bending zone 1, as well as core damages in bending and shear in zone 2, monitored by IRT and AE simultaneously. All sandwich specimens have two identical symmetrical skins made of 3-layer GFRP balanced fabric/epoxy oriented in the warp direction (Ref: Sicomin glass twill 3190 with 190 g/m², with 50% fiber volume fraction). The core is made from balsa wood (Ref: BALTEK SB.100). Material parameters of the skin and balsa core can be referred to Wu Y et al., 2021.

Five wet GFRP-balsa sandwich specimens were firstly dried in the oven under 40 ℃ and then immersed into water under room temperature to get saturated moisture content (MC) of 120% after nearly 4 months. And then, wet and dry sandwich specimens were tested under the same loading condition, controlled by displacement rate imposed at 2 mm/min (ASTM C393) using a MTS machine with load cell of 100 kN (see Fig. 1). The loading span (L) is 80 mm, and the support span (S) is 240 mm. Two AE wideband sensors with a sensor distance of 180 mm were fixed symmetrically on the upper surface of the specimen (see Fig. 1. (b)), to monitor all the possible damages during bending tests. The threshold was set by 28 dB. The pre-amplifier is 40 dB, and the analog-filter is in the range of 20 kHz -3 MHz. Peak Definition Time (PDT)

is 30 µs, Hit Definition Time (HDT) is 100 µs and Hit Lockout Time (HLT) is 300 µs. All the parameters have been validated by preliminary tests in Wu Y et al., 2021. IRT system was set to mainly monitor the upper skin damages in zone 1 (see Fig. 1. (c)), including IR camera (FLIR X6801sc, with a resolution of 608 × 312 full images at 520 frames per second) and acquisition computer with ResearchIR Master software.

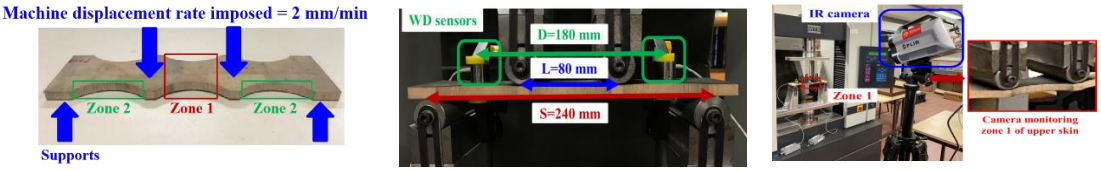


(a) Loading condition (b) AE wideband sensors (c) IR camera setup

Fig. 1: 4-point bending test configuration monitored by IRT and AE

## 3. Results and discussions

### *3.1. Moisture effects on static 4-point bending behavior of GFRP-balsa sandwich*

Force/Displacement curves of wet (MC=120%) and dry sandwich specimens were compared in Fig. 2. All the specimens show a similar linear behavior before the final sudden rupture. Compared to dry sandwich, the average bending stiffness of wet specimens at loading points shows about 19% decrease, from 108 N/mm (±3 N/mm) to 88 N/mm (±3 N/mm). The average fracture load of wet ones (730 N±37 N) is about 35% lower than that of dry ones (1115 N±100 N). It proves that moisture has caused obvious decrease of bending stiffness and strength.

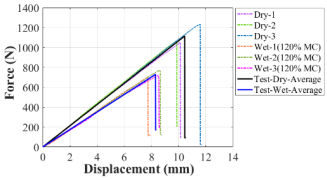


Fig. 2: Moisture effects on static 4-point bending behavior of GFRP-balsa sandwich

Post-mortem examinations of zone 1 using microscope VHX-7000 (100 X) were investigated for both wet and dry specimens. Fig. 3. (a) -(b) show the final upper skin surfaces of dry and wet sandwich, while Fig. 3. (c) -(d) show the side skin/core surfaces. There are some fiber/matrix extensions on the skin surface, released by very rapid high energy of dry sandwich (see Fig. 3. (a)), but this phenomenon could not be seen on wet specimens. In Fig. 3. (c) -(d), skin/core debonding crack of dry specimen is longer and wider than that of wet one, but skin delamination of wet specimen is more obvious. Core cracks of wet specimen are more severe in Fig. 3. (d), while dry specimen almost has no core damage. So, moisture absorption could cause more severe skin delamination and core damages, but less severe skin/core debonding and fiber breakage.


(a) Skin damages of dry specimen (b) Skin damages of 120% MC specimen

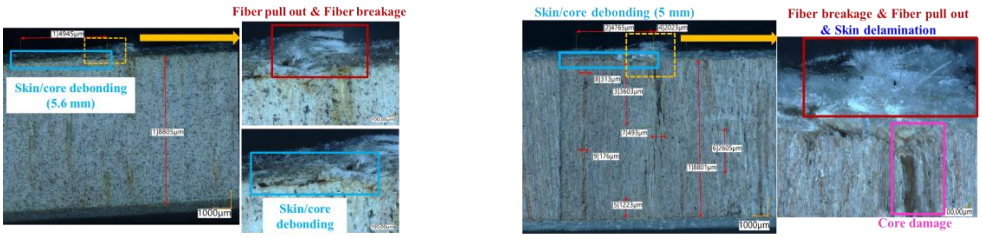


(c) Skin/core damages of dry specimen (d) Skin/core damages of 120% MC specimen

Fig. 3: Microscopic images of damages of dry and wet GFRP-balsa sandwich

*3.2. Damage initiation detection by AE*

AE amplitude is the most often used AE time parameter (Perrin M et al., 2019) to be correlated with damage mechanisms of composite and wood structures. Fig. 4 shows that AE amplitude accumulation of wet and dry specimens experiences a similar tendency to Force/Time curve, which increases intensely just before the final fracture load. The highest amplitude values of dry and wet specimens are 98 dB at 353 s and 92 dB at 257 s. Highest AE amplitude higher than 90 dB could be fiber breakage (Munoz V et al., 2016) of composite laminates. It could indicate that fiber breakage of wet specimens occurs for lower stress level compared to dry ones.

AE hits appearing before the onset of skin delamination are lower than 60 dB for all specimens, which could be dominated by resin cracking (Munoz V et al., 2016) of the skin. Hits between 30-60 dB increase for wet specimen at the beginning of the tests, combined with microscope observations, these signals may be caused by small core cracks, but this requires further experimental investigations.


(a) Dry sandwich (b) Wet sandwich (MC=120%)

Fig. 4: Moisture effects on AE amplitude distributions of GFRP-balsa sandwich

*3.3. Damage initiation and evolution observations by IRT*

2D heat diffusion equation (see Eq. 1) was used to determine the heat source field during the damage evolution process, by considering the dependence of temperature data on time and space simultaneously (Munoz V et al., 2016). The heat source s contains the irreversible mechanical dissipation $d_1$ and the reversible thermoelastic coupling $s_{the}$ between the temperature and strain; $\Delta T = T - T_0$, which is the temperature difference; $T_0$ is the average temperature of the first ten IRT images; $T$ is temperature at time t; $\rho$ is density; $C$ is specific heat; $k$ is the thermal conductivity coefficient. Correlation between movement of the vertical pixel in IRT temperature images and true displacement of the specimen was introduced into MATLAB program to improve the accuracy of post-processing of thermal images by $\Delta T=T_1-T_0 + T_2-T_1+\ldots+ T_t-T_{t-1}$.

$$\rho C \frac{\partial \Delta T}{\partial t} - k\left(\frac{\partial^2 \Delta T}{\partial x^2} + \frac{\partial^2 \Delta T}{\partial y^2}\right) = s \quad (1)$$

The cumulative irreversible damage $D_1$ can be calculated by Eq. (2):

$$D_1 = \int_0^t d_1 \, dt \quad (2)$$

Fig. 5-6 show the cumulative heat source images during the tests. What's interesting was that some small heat source extensions appearing in the air in red circles around the specimen have been captured by IR camera in Fig. 5. (b). It should be caused by dynamic effect of higher energy released very rapidly, consistent with microscope observations in Fig. 3. (a). In Fig. 6. (a)-(c), IRT could observe more clearly the damage initiation point and propagation path of wet sandwich. It shows that wet and dry sandwich experience a similar damage evolution process, but skin cracks of dry sandwich (1.04 s) propagate much faster than the wet one (1.55 s). Fig. 5. (c) and Fig. 6. (c) show the final skin cracks at the end of tests, showing good agreement with the damage photos in Fig. 5. (d) and Fig. 6. (d).

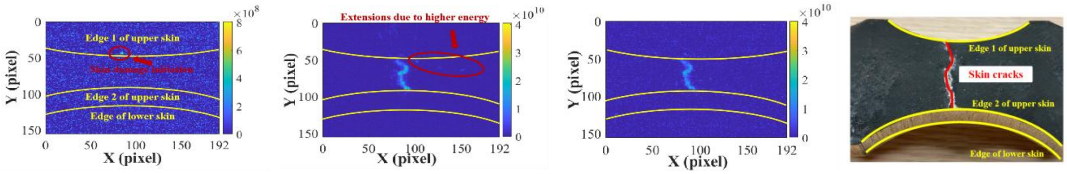


(a) t=350.36 s (b) t=351.37 s (c) t=351.40 s (d) Final fracture surface

Fig. 5: Cumulative heat source (J/m$^3$) images and damages of dry GFRP-balsa sandwich

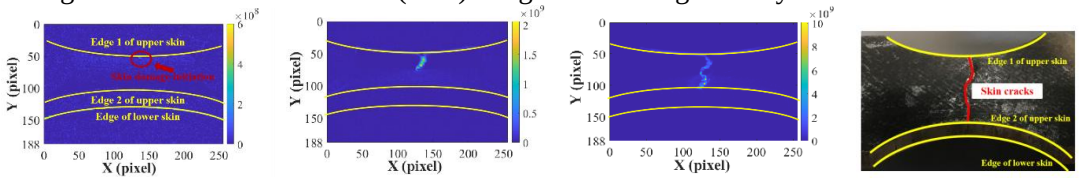


(a) t=255.43 s (b) t=256.94 s (c) t=256.98 s (d) Final fracture surface

Fig. 6: Cumulative heat source (J/m$^3$) images and damages of wet GFRP-balsa sandwich

## 4. Conclusions

In this work, post-mortem microscope observations were correlated with AE and IRT monitoring during 4-point bending tests to investigate moisture effects on damage mechanisms of GFRP-balsa sandwich. It was found that moisture absorption could cause the reduction of bending stiffness and strength of the sandwich specimen, as well as the more severe GFRP skin delamination and balsa core damages. However, skin/core debonding and fiber breakage of wet sandwich were less severe. These conclusions contribute to the application of balsa wood as core materials in composite sandwich structures in aviation and marine industries.

## References

Wu Y, Perrin M, Pastor M L, Casari P, Gong X. (2021) On the determination of acoustic emission wave propagation velocity in composite sandwich structures, Composite Structures, 259, 113-231.

Shi H, Liu W, Fang H. (2018) Damage characteristics analysis of GFRP-Balsa sandwich beams under Four-point fatigue bending, Composites Part A: Applied Science and Manufacturing, 109, 564-577.

Da Silva A, Kyriakides S. (2007) Compressive response and failure of balsa wood, International Journal of Solids and Structures, 44(25), 8685-8717.

Munoz V, Valès B, Perrin M, Pastor M L, Welemane H, Cantarel A, Karama M. (2016) Damage detection in CFRP by coupling acoustic emission and infrared thermography, Composites Part B: Engineering, 85, 68-75.

Perrin M, Yahyaoui I, Gong X. (2019) Acoustic monitoring of timber structures: Influence of wood species under bending loading, Construction and Building Materials, 208, 125-134.